# Microcrystalline Cellulose Isolation – Proposed Mechanism: Enhanced Coupling

Miguel Ángel García Hernández,[a] Arturo López Marure,[a,*] María Guadalupe Neira Velázquez,[b] Jaime Alfredo Mariano Torres,[c] and Adrian Arroyo Galvan [a]

Cellulose-derived materials are an emergent opportunity for reducing the environmental impact of polymers. Microcrystalline cellulose (MCC) has increasing relevance in many sectors, including pharmacy, food, and reinforcement of polymers, but its application is limited by the low coupling between it and nonpolar polymers and the polar behavior of cellulose derivates. There is not a well-defined model for the isolation of MCC and the factors involved in the length and width, which are elements of high influence on the reinforcement effect of MCC. This study proposes a mechanism for the size reduction of cellulose fibrils isolated through acid hydrolysis and a post-plasma surface modification (PSM) to enhance coupling of the MCC with hydrophobic polymer matrixes. MCC was characterized by FTIR, XRD, and SEM before and after the plasma surface treatment with caprolactone, a biodegradable polymer. There were no changes in the FTIR spectra; however, in XRD the sample exhibited a decrease in intensity. These results suggest that PSM did not change the structure of MCC or chemical composition. However, an increase in the peak temperature of degradation confirmed the surface modification of MCC.

*DOI: 10.15376/biores.18.1.1788-1802*

*Keywords: Microcrystalline cellulose; Plasma surface modification; Biopolymer; Renewal resources*

*Contact information: a: Instituto Politecnico Nacional, CICATA ALTAMIRA. Carretera Tampico-Puerto Industrial Altamira, Tamaulipas CP, 896000, Mexico; b: Centro de Investigación en Química Aplicada, Blvd Enrique Reyna 140, Cp, 25253, Saltillo, Mexico; c: Universidad del Noreste, Av. Miguel Hidalgo 6315, Nuevo Aeropuerto 89337 Tampico, Mexico; * Corresponding author: arlopezm@ipn.mx*

## INTRODUCTION

Cellulose is the most abundant biological material on the planet. It is found in all superior plants, and it is synthetized by bacteria and urochordates. In plants it provides structural support in the cell wall. Cellulose is a semi-crystalline natural biopolymer conformed by repeating units of d-glucopyranose bonded by beta glycosidic linkage between C1 and C4. Cellulose and their derivates are an alternative to replace the oil-based polymers on account of their good mechanical properties, low density, biocompatibility, and biodegradability; these useful properties justify many practical applications of cellulose derivatives in diverse fields. However, there are limitations in cellulosic materials, *i.e.*, the hydrophilic behavior of cellulose makes it difficult to incorporate cellulose derivates in a polymeric matrix. Such problems result in a detriment in the potential effect of reinforcement (Trache *et al.* 2016). In previous work, acid hydrolysis was used to isolate MCC from cotton sliver. The procedure provided microcrystalline cellulose that was less thermally stable compared to commercial MCC. The MCC isolated showed more hydrophilic behavior because of the introduction of sulphate groups onto the

surface (Kale *et al.* 2018). To solve this problem, surface modification has been applied to cellulose derivatives before the incorporation onto the polymeric matrices. There are many ways to accomplish that, but one of the most interesting of these procedures is plasma surface modification (PSM), whereby a thin deposit of an organic precursor is bonded to the MCC surface to enhance compatibility with the matrices and reinforced mechanical or thermodynamic properties.

MCC is a modified material obtained from depolymerized cellulose; it is usually prepared by acid treatment of alpha cellulose, a derivate of the raw cellulose without any other of the natural biopolymers of intrinsic present in plants (lignin, hemicellulose). Acid hydrolysis has some drawbacks. Commonly it uses sulfuric acid; the procedure decreases the coupling between cellulose derivates and host polymers matrix because of the residual sulfation on the surface. However, there is no detailed mechanism for the size reduction and the elements involved in the isolation of MCC and their influence on the mechanical properties of the material, such as reinforcement in polymer composites. In the reinforcement of polypropylene with MCC, the composites were prepared with poly(polypropylene-graft-maleic acid) and MCC with silicone oil, stearic acid, or alkytitanate like coupling agents. The thermal stability of the matrix was poorly enhanced. The temperature of crystallization of the matrix and the modulus of the composite increased with increasing MCC content, confirming an effective filler effect that allowed greater stress transfer (Spoljaric *et al*. 2009).

The synthesis of bio-composites based on MCC isolated by acid hydrolysis has been studied, and the mechanical properties of these composites show an important improvement in the tensile strength of 37.7% at 20% w/w. Additionally, at that concentration good thermal stability is obtained for processing and thermoforming (Crews *et al*. 2016; Ponsuriyaprakash *et al.* 2020). However, fracture analysis brings information about the consolidation of the composite, and the reinforcement phase was pulled out of the matrix, a sign of poor coupling between them. The reinforcement of thermoplastic matrix with different cellulose derivates is an important research line; in fact, there are more works with cellulose derivates at nanoscale such as nanocrystals (cellulose nanocrystals) and some of them with enhanced coupling. This is the case of the composite of ABS and nanocellulose isolated by acid hydrolysis (nanowhiskers) synthesized by melt mixing (Leão *et al.* 2020). The synthesis resulted in a material with significantly enhanced mechanical properties, depending on the particle dimensions *i.e.*, with shorter length the tensile strength was improved, and with longer length the impact force was enhanced with a detriment in tensile strength. In general lines, the coupling limit of the reinforcement phase calls attention to the low interactions among the composite components (Leão *et al.* 2020).

The incompatibility of cellulose with commonly used synthetic polymers is a well-identified problem. Plasma surface modification, an environmentally friendly technique, was used in recent research to increase the coupling of cellulose nanocrystals isolated by acid hydrolysis with ABS in bulk polymerization. The composites with the reinforcement phase modified with plasma showed better results. An increase was noticed in the viscosity. This was attributed to a movement restriction of the polymer chains of the matrix by the nanocrystals, showing more interactions than the composites without the plasma surface modification. That procedure involved the deposition of a plasma polymer onto the surface. The mechanical characterization showed an increase of 117% of the impact strength and good interaction in the rheology interpretation of results (Alanis *et al.* 2019).

In this research, a mechanism is proposed for the size reduction throughout the isolation process, taking account of almost all the variables involved in the acid hydrolysis. The idea is that if this phenomenon can be better understood, it will then be possible to make better use of this important and emerging material in the revolution of renewable material with the most important engineer thermoplastics with an enhanced coupling by the PSM for the synthesis of hybrid composites.

## EXPERIMENTAL

### Materials

Alpha-cellulose (SC-214443), ε-caprolactone (502-44-3), sulfuric acid ($H_2SO_4$ 7664-93-9), deionized water (OCAA00) and sodium hydroxide (NaOH 1310-73-2) was purchased from Sigma Aldrich.

### Acid Hydrolysis

First, 10 g of alpha-cellulose was isolated by acid hydrolysis with $H_2SO_4$ in a relation of 1:20 at 54 % with heating (45 °C) and stirring for 1 h (Trache *et al.* 2017). The reaction was quenched in an ice bath until the heat was dissipated. This was followed by washing with deionized water until the solution reached pH 4. Then centrifugation was carried out at 3500 rpm for 10 min. Drops of sodium hydroxide (0.1 N) were added to the suspension to neutralize it. The neutralized suspension was sonicated using a bath sonicator at 60% output for 30 min. The solvent was extracted in a vacuum oven at 100 °C for 1 h. (Oh *et al.* 2005).

### Plasma Surface Modification

The plasma surface modification is based on plasma polymerization and was done in a lab-made reactor consisting of 3 main systems. The first one is the reaction chamber: a 500 mL Pyrex glass flask where the plasma polymerization takes place. The procedure starts with the evaporation of an organic precursor (caprolactone), followed by its transformation to a high energy state that favors the formation of free radicals. In the last stage of this procedure, free radicals condense in a thin coating onto the surface. The apparatus is connected to a rotary evaporator, acting like a connection between the reactor chamber and the other parts of the reactor and providing agitation.

The gas delivery system is the second main component of the reactor. It consists of a Schlenk tube containing the organic precursor connected to the rotary evaporator through a hose and a regulated gas valve. The last main component of the reactor is the electrical excitation system, formed by a radiofrequency generator connected to two electrodes. One of them is a copper wire coiled around the glass flask.

The reaction starts with 1 g of MCC deposited onto the glass flask. This was put under vacuum until reaching a pressure of $1.5 \times 10^{-1}$ mbar. After that, the organic precursor was introduced, and it flowed until achieving a stable pressure of $2.5 \times 10^{-1}$ mbar. The radiofrequency generator started to work after the organic precursor was added to the reactor at a frequency of 13.56 MHz (Fig. 1). In this case, the organic precursor was ε-caprolactone. This was selected because of its good results in enhancing coupling in hybrid composites based on cellulose derivatives (Alanis *et al.* 2019).

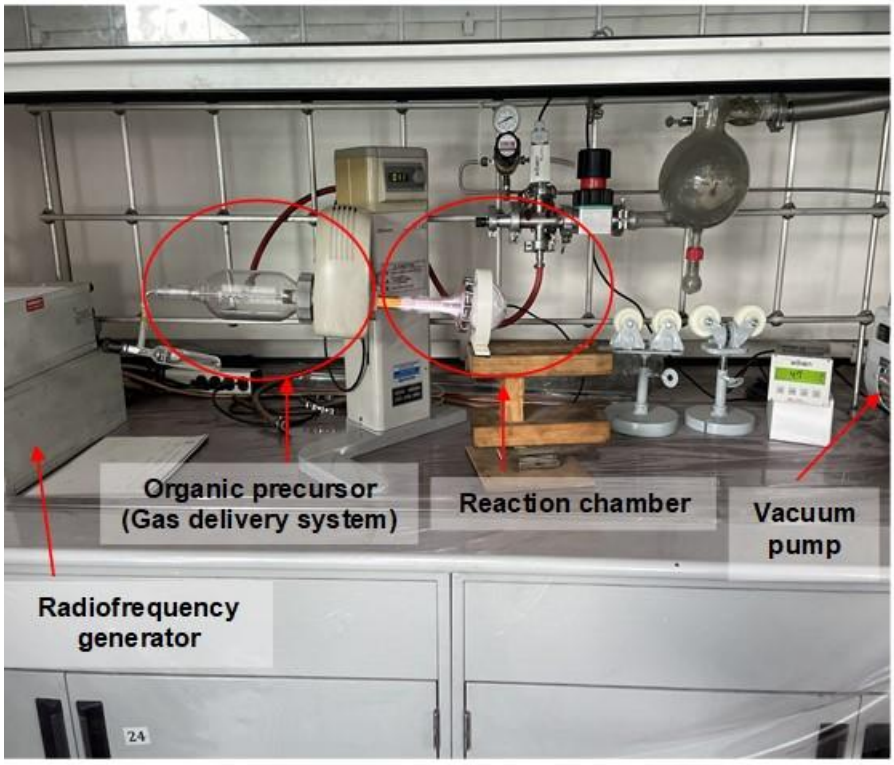


**Fig. 1.** Lab-made plasma reactor

## Characterization Before and After PSM

Fourier transform infrared spectroscopy (FTIR) was performed in a Spectrum One device (Pelkin Elmer, Mexico City, MX) with 8 scan number, with 4 $cm^{-1}$ in the range of 450 to 4000 $cm^{-1}$. X-ray diffraction (XRD) was carried out in a Bruker D8 (Bruker Mexicana, Mexico City, MX) Advance Vantec with step size of 0.02°, $2\theta$ range: 5° to 40° and voltage of 40 kV. Scanning electron microscopy (SEM) was performed in a Jeol, JSM-6390LVat (JEOL Mexico City, MX) at 80 kW voltage acceleration. ANOVA analysis was performed on 500 particles measured from 8 images for each sample. Thermogravimetric analysis (TGA) was performed in a TA Instrument 5500 equipment (TA Instruments New Castle, USA) using a heating ramp of 10 °C/min in an analysis range of 30 to 800 °C under an atmosphere of $N_2$ until 600 °C, after which the atmosphere was changed to $O_2$.

## Relative Degree of Crystallinity

The relative degree of crystallinity (CI) was calculated using Eq. 1, where $I_{min}$ is the minimum at 18° of $2\theta$ and $I_{max}$ is the intensity of the peak at 22°. The 18° corresponds to the amorphous region of MCC, and the 22° is relative to the crystalline phase of the material. This method is used to determine the proportion of periodic zones in MCC using the diffraction peak of crystallinity zones and the minimum of amorphous regions. It is a relative degree because this analysis is qualitative (Segal *et al.* 1952; Kale *et al.* 2018; Kerche *et al.* 2022).

$$I_{ic} = \left(1 - \frac{I_{min}}{I_{max}}\right) 100 \quad (1)$$

## RESULTS AND DISCUSSION

There were 2 samples of cellulose with variations on parameters of extraction (Table 1) to make a comparative of the influence of these parameters in the size reduction. For the first sample (C1), the sonication time was 10 min. After the first results of characterization, the sonication time was adjusted to 30 min. The MCC was dried in a vacuum oven at 100 °C for 1 h.

**Table 1.** Experimental Matrix

| Acid solution (%) | C1 | C2 |
|---|---|---|
| Cellulose (g) | 10 | 10 |
| pH | 6 | 7 |
| Neutralization with NaOH (M) | N/A | 0.1 |
| Centrifugation (rpm) | 3500 | 3500 |
| Washing (min) | 10 | 10 |
| Ultrasonication (min) | 10 | 30 |
| Dry (°C) | 100 | 100 |
| Dry (H) | 1 | 1 |

### X-Ray Diffraction of MCC

The acid hydrolysis produces cellulose type 1, with diffraction peaks at 16°, 22°, and 34.6° (Morán *et al.* 2008; Sèbe *et al.* 2012; Huang *et al.* 2019). The peak at 22° is attributed to the periodic phase on the cellulose materials.

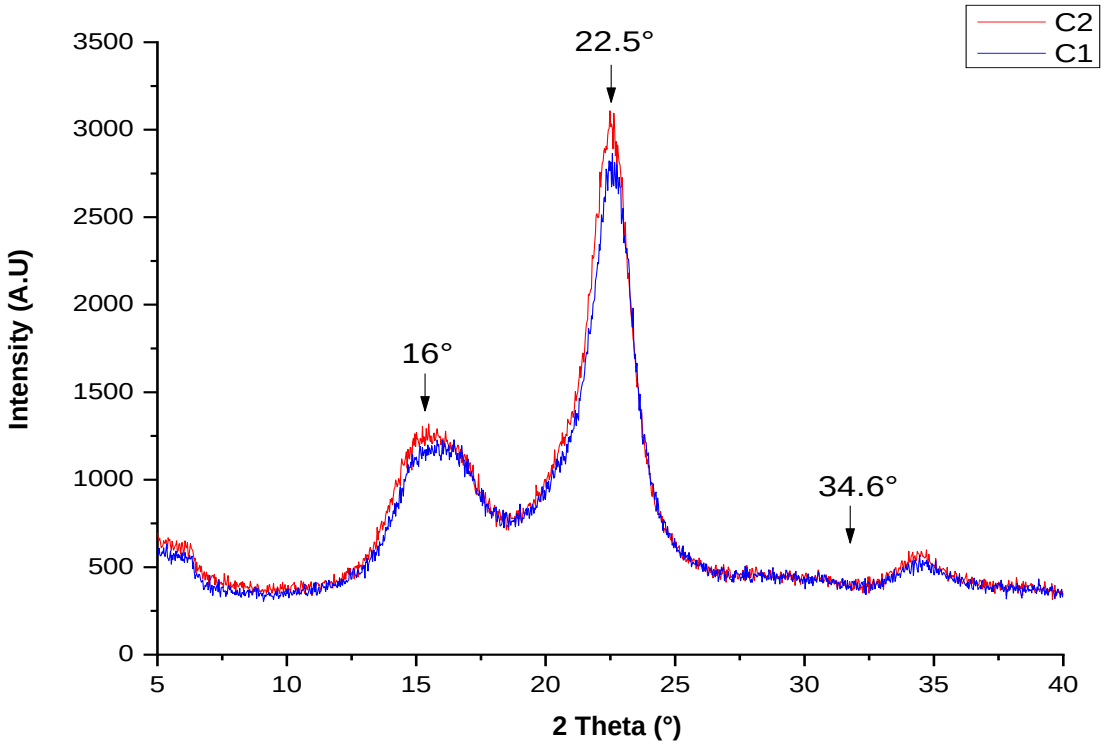


**Fig. *2.*** XRD Spectra of C1 and C2

In C2 there was an increment in intensity of the peak at 22°. This parameter indicates that C2 had more periodic regions. The material corresponded to a semicrystalline

solid. Samples C1 and C2 had a crystallinity index of 73%, and 75%, respectively. The changes in the relationship of periodic and amorphous regions can be attributed to two elements related to thermal factors of extraction. C2 was neutralized with NaOH, and according to the literature, acid hydrolysis with $H_2SO_4$ decreases the thermal resistance of the MCC due to residual sulfation on the surface. The neutralization brought more resistance to heat and that explains the sharp and higher peak of 22° in C2 (Oun and Rhim 2015) (Fig. 2).

## FTIR

At 896 $cm^{-1}$ there was an absorbance band related to stretching vibrational mode of the glycosidic linkage between the monomeric units of glucopyranose that conforms the polymer (Trilokesh and Uppuluri 2019). The band at 1028 $cm^{-1}$ corresponds to the pyranose ring; this structure is the skeleton of the monomeric unit in a stretching vibration mode. An absorption band at 1028 $cm^{-1}$ corresponds to the secondary alcohols on the carbons 2 and 3 of the monomeric unit in a stretching vibrational mode (Espino-Pérez *et al.* 2013). The absorbance band at 1160 $cm^{-1}$ is related to C-O-C bond in a wagging vibrational mode.

One of the most characteristic absorption bands of cellulose derivatives was observed at 1430 $cm^{-1}$ corresponding to C-$H_2$ linkage in a symmetric flexion (Alanis *et al.* 2019; Pambudi *et al.* 2021). The $H_2O$ absorbed in the sample shows their absorbance band at 1641 $cm^{-1}$. The last two absorbance bands detected were at 2897 and 3336 $cm^{-1}$ corresponding to C-H stretching vibrational mode and primary alcohols in symmetrical stretching vibrational mode (Pambudi *et al.* 2021) (Fig. 3).

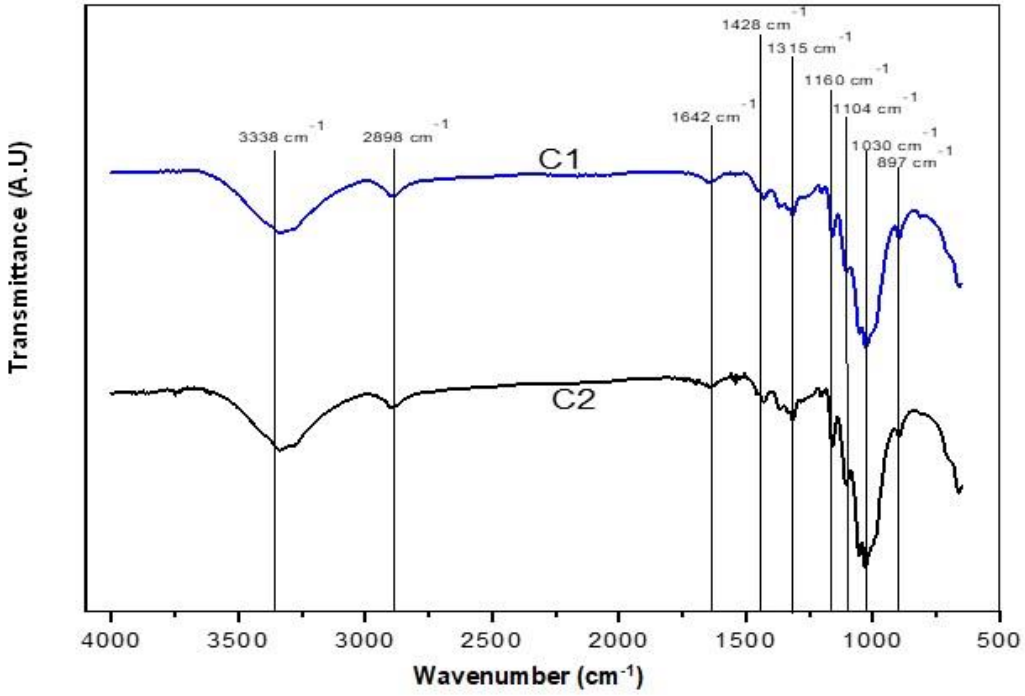


**Fig. 3.** FTIR Spectra of C1 and C2

In C2, drops of NaOH solution were added until neutralization. There was no specific absorbance band observed for this compound, which could be because of the range of analysis of the equipment (500 to 4500 $cm^{-1}$). According to the literature, the absorbance bands of NaOH are near to 5000 $cm^{-1}$. The sample C2 was dried at 100 °C, which involves

a degradation of amorphous regions of less thermic resistance. That explains a sharp peak on the XRD spectra at 22° and agglomeration on the MCC particles, visible on the changes of FTIR spectra where the absorbance band corresponding to the water on the sample shows higher absorbance. The NaOH reacted with the sulfates groups formed on the surface bringing $H_2O$ as by-product.

The agglomeration of MCC by thermic drying is a factor in all cellulose derivatives in a well understood mechanism of 3-step kinetic evolution (Fig. 4). However, the growth in size due to the agglomeration of MCC particles improved thermal resistance and an increase in the peak degradation temperature. In the first stage, the decrease of suspension volume and the increase in the capillarity forces moves the particles when the water evaporates. In the second stage, the surface of particles is exposed by vapor diffusion of the water molecules, then the capillarity forces reach their maximum level, shortening the distance between MCC particles. In the third stage, the velocity of water transfer is higher than vapor diffusion velocity and promotes the molecular contact between MCC particles (Peng *et al*. 2012). Finally, the energy transfer to the suspension gives enough energy for the formation of hydrogen bonds. This mechanism gives particles of bigger size, far from the nanoscale. The particles of bigger size had higher thermal resistance, *i.e*., the particles drying by heat can be a better option for applications such as fused deposition or extrusion without structural damage in the material.

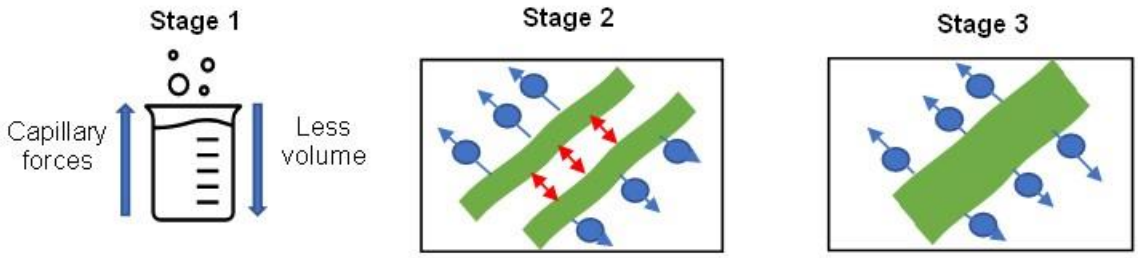


**Fig. 4.** Agglomeration mechanism of heat drying

## SEM

MCC had the form of a thin ribbon. In C1 (Fig. 4) the particles had inhomogeneous dimensions (length) with a standard deviation of 102 µm. In C2 (Fig. 5), the standard deviation was 45 µm. According to previous studies, a homogeneous distribution of dimensions will be a desirable factor to enhance the adhesion mechanism, helping the diffusion of particles and avoiding possible agglomeration on the final composite. The micrographs of C1 exhibited some agglomeration of MCC particles and some amorphous regions that were not hydrolyzed; these non-hydrolyzed regions will not interfere with the composite synthesis because of their low presence in MCC. The MCC of C2 (Fig. 6) had fewer agglomerated regions and showed more fragmentation of polymeric chains. Possibly, the cavitations generated on the sonication bath improved the cleavage of it. The length of MCC particles is inversely proportional to the sonication time (Qiao *et al.* 2016).

The morphological analysis brings relevant information about the benefits or side effects of defects onto the surface of particles. In this case, MCC showed fewer deep defects, like stretch marks and fissures. These types of defects can be a reinforcement on the mechanical interlocking, where fewer deep defects provide keying sides to start the interdiffusion of polymeric chains between the matrix and the reinforcement. More severe defects such as cracks promote the catastrophic breakage of the particle (González-Velázquez 2021).

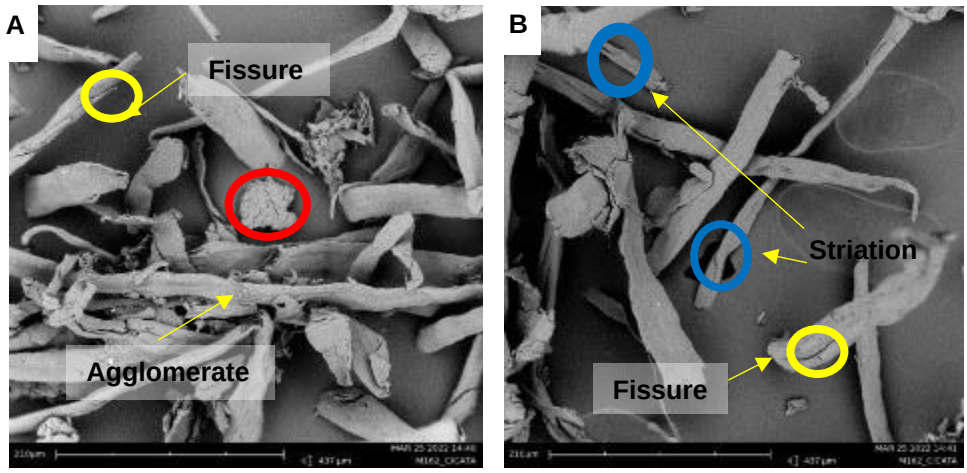


**Fig. 5.** MCC micrographs of C1; stretch marks (blue), fissures (yellow), and cracks (red)

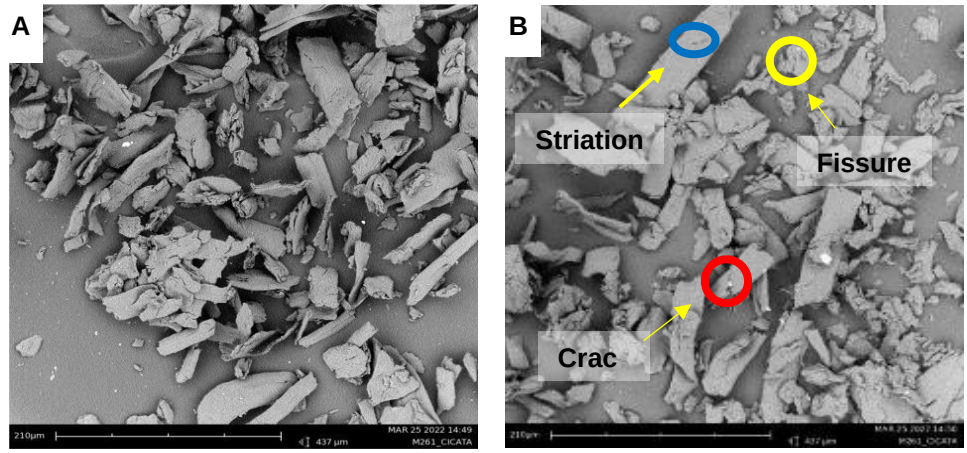


**Fig. 6.** MCC micrographs of C2; stretch marks (blue), fissures (yellow), and cracks (red)

## Thermogravimetric Analysis of MCC

Two stages of decomposition were observed for MCC. The first stage at approximately 40 °C corresponded to the water absorbed and compounds of low molecular weight. The second stage started at approximately 240 °C, and it corresponded to the degradation of macromolecular chains of MCC. In C1 (Fig. 7) the first decomposition stage started early at 37 °C because of the low thermal resistance due to the sulphate groups onto the surface of MCC. However, sulphate groups act as a flame retardant because of the formation of ash on the surface. The peak temperature of degradation (PTD) was 318 °C, which is lower than alpha cellulose; thus, the thermal degradation of this sample is faster because of the presence of sulphate groups. In C2 (Fig. 8) the first stage of degradation started at 47 °C and the second stage near to 240 °C. The PTD improved to 327 °C. This finding confirms the enhanced thermal behavior of the neutralization with NaOH. However, the salts derived from NaOH formed carbonized material and that protected some material from thermo-oxidation. At the end of the analysis, 20% of the material remained. Thus, the neutralization improved the thermal resistance of MCC without detriment to the flame-retardant property.

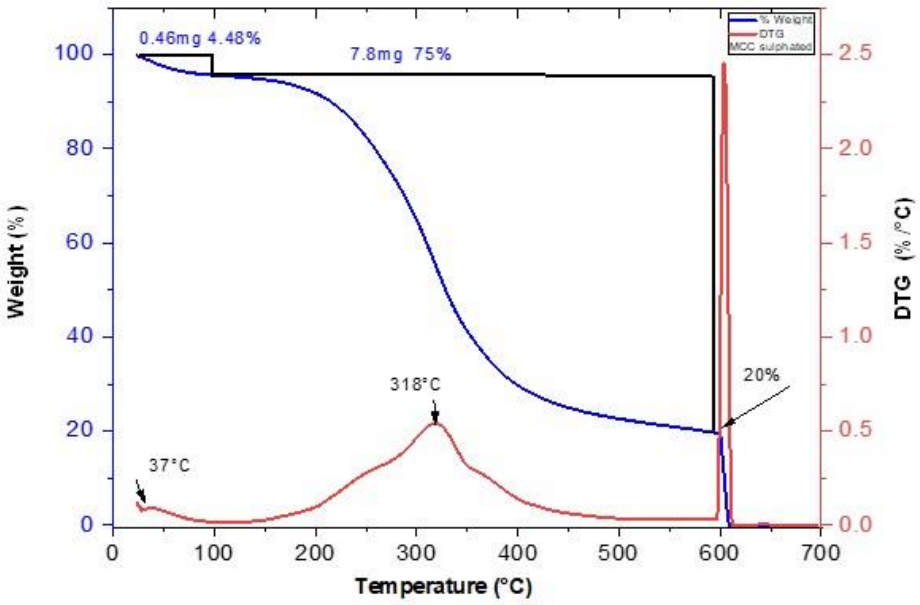


**Fig. 7.** Thermogravimetric analysis C1

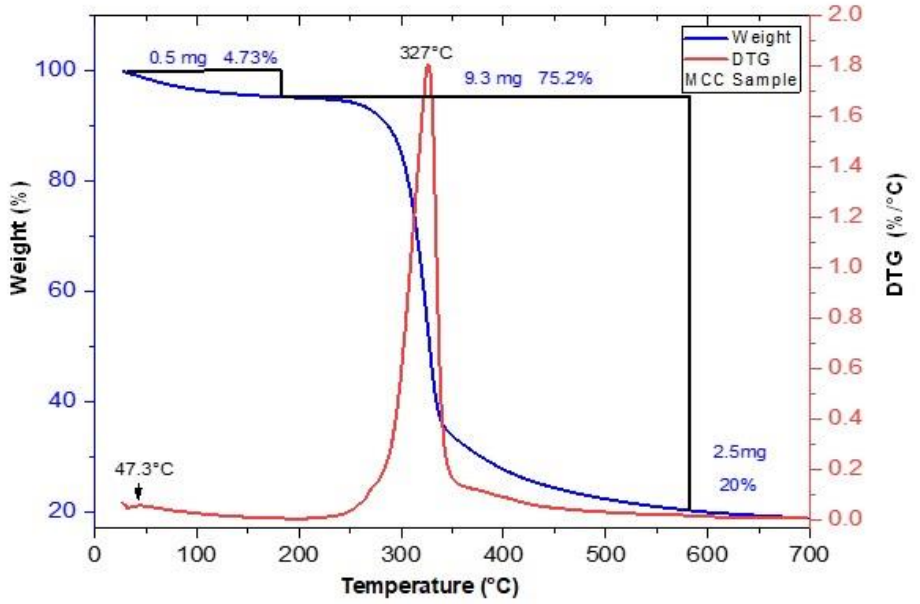


**Fig. 8.** Thermogravimetric analysis C2

## Proposed Fracture Mechanism

The parameters of MCC isolation influence the particle size. The comparative results of the modification on the procedures makes it possible to discern the kinetic evolution of the cleavage of MCC particles. This phenomenon starts with acid hydrolysis, where the acid acts like a catalyst apporting hydronium ion. Those ions react selectively with the glycosidic linkage with the oxygen molecules, starting a protonation. The cleavage in this mechanism is based on the Pauli exclusion principle, where two particles of the same quantum number cannot exist on the same system, and it generates repulsion between ions and the bonds because the superposition on the wave function causing electrostatic

repulsion. This effect acts like a shear stress, operating on the ends of the particle, exerting torsion on it until it breaks. The dimensions of the particles after the acid hydrolysis show nonhomogeneous dimensions.

The phenomenon of cavitation acted in an efficient way to distribute particles in response to the constant energy provided to the system, thereby reducing the standard deviation of sizes in MCC. The ultrasonication provides high pressure waves that induce the formation of bubbles on the surface of MCC particles in the interface solid-liquid (Mørch 2015). The biggest particles will interact with more cavitation, and at a certain moment, the mass transfer will bring particles of near dimensions, releasing energy and causing fragmentation. Theoretically, in some moment the particles could experience a similar number of cavitations, approaching the dimensions to homogeneous dimension of the particles (Fig. 9). That element can be observed as a reduction of standard deviation of length (Shaik *et al.* 2005, 2009; Wu *et al.* 2009; Peng *et al*. 2012; Voronova *et al*. 2012).

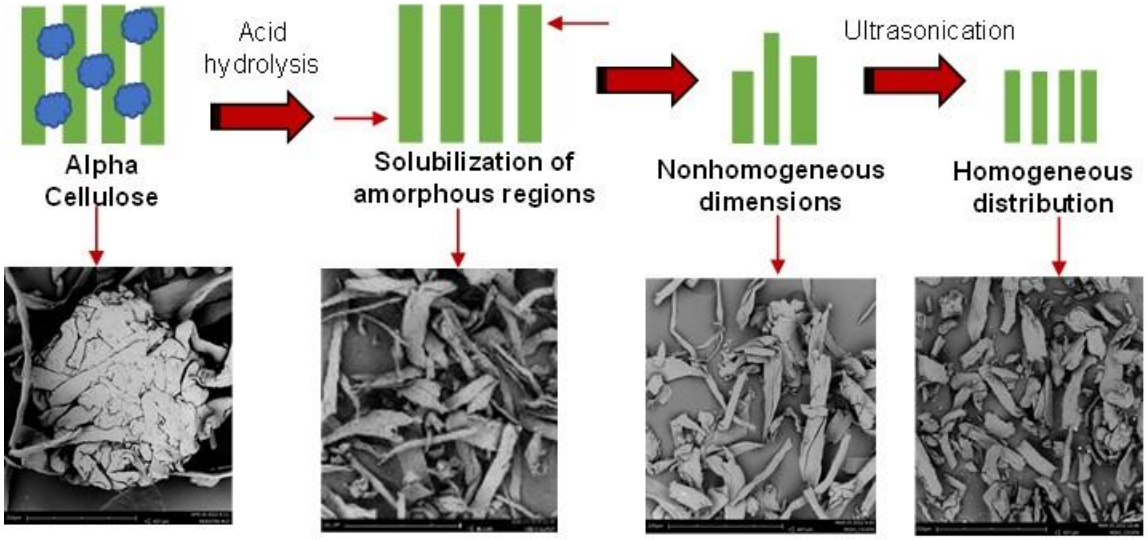


**Fig. 9**. Proposed Mechanism for size reduction of MCC

## FTIR Analysis after Surface Plasma Modification of MCC

There were some changes in the intensities of the FTIR spectra of the samples The plasma surface modification used the phenomenon of plasma polymerization. Where an organic precursor undergoes a process of fragmentation, recombination, and condensation. In the recombination stage, particles were guided by dipolar momentums and the orientation was a function of the electromagnetic field that promotes cleavage of polymeric chains. In the last stage, the reactive species formed in the recombination stage condensed in a thin coating on the surface of MCC. However, there were no new absorbance bands related to the organic precursor. These results suggest there were not any changes in the functional groups that could interfere in the synthesis of hybrid composites (Fig. 10).

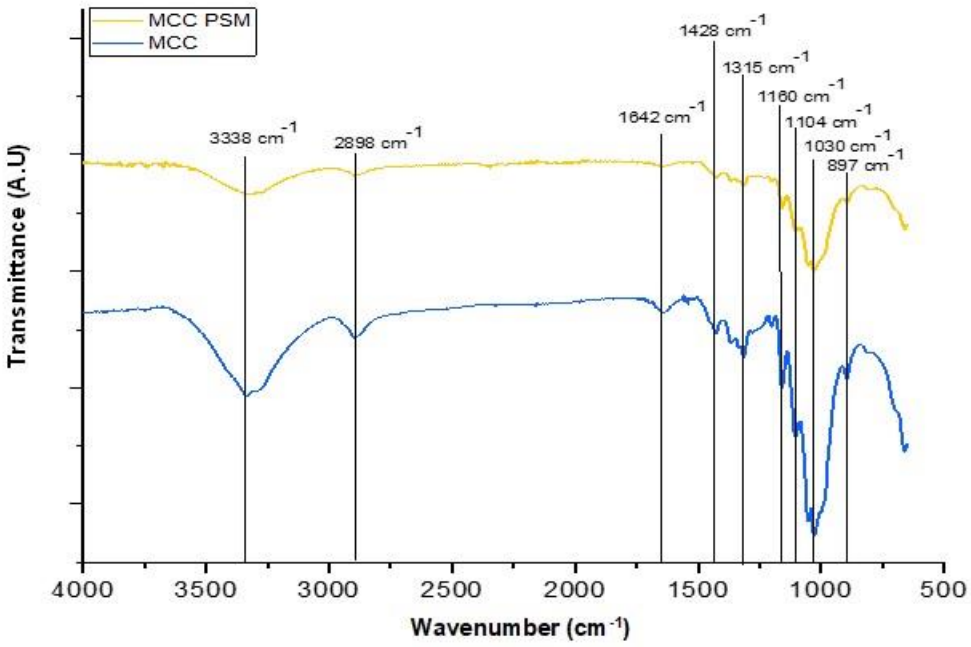


**Fig. 10.** FTIR spectra MCC and MCC PSM

## XRD Analysis after Plasma Surface Modification of MCC

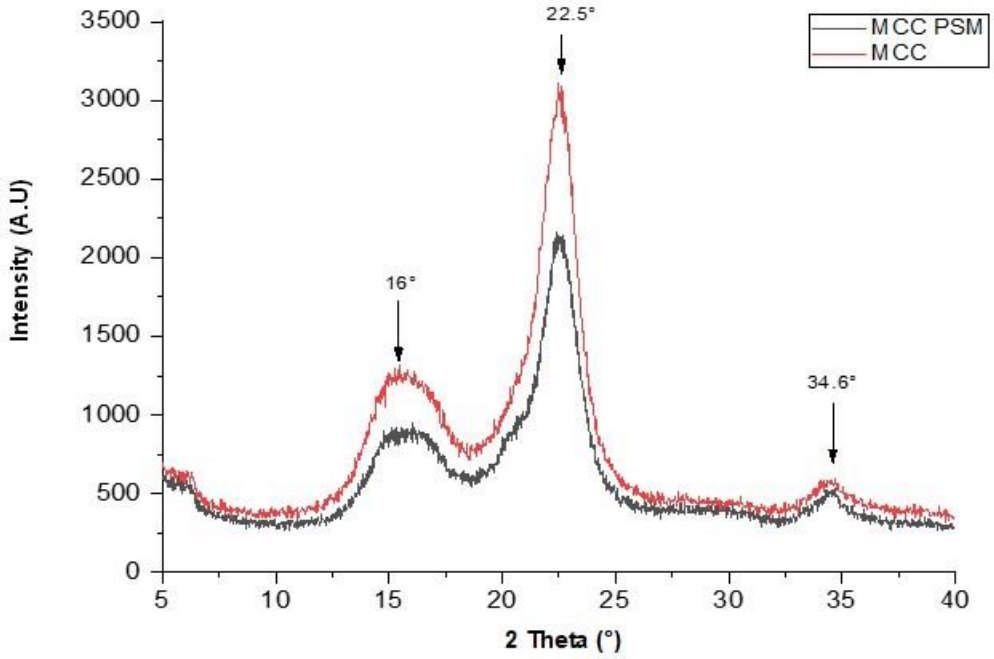


**Fig. 11**. XRD spectra MCC and MCC PSM

After the plasma surface modification, there were no new diffraction peaks; however, the sample showed less intensity on all the peaks previously detected for MCC. The decrease in the diffraction peaks is a signal of reduction of the periodic regions of MCC. Thus, the MCC after plasma surface modification showed changes in the amorphous zones. In particular, there was an increase in the qualitative detection of it. Probably the

reduced crystallinity can be attributed to deposition of irregular sections of polycaprolactone. Otherwise, in the first stage of plasma surface modifications the ions bombard the surface accelerated by the plasmatic sheath, modifying the morphology of the particles. The loss of periodicity is not a desirable factor in the synthesis of composites (Trache *et al.* 2016). However, according to previous work with PSM, in this case the reduction of crystallinity it could not be a limitation of MCC in the synthesis of polymer composites because the crystallinity remains similar to MCC without PSM (Alanis *et al.* 2019) (Fig. 11).

## Thermogravimetric Analysis after Plasma Surface Modification

After PSM, the first stage of degradation started at 38 °C. The second stage of degradation was related to macromolecular chains of MCC. The PDT improved to 349 °C and the solid remanent decreased to 10.7%.

The flame-retardant property was lost after the plasma coating; however, the PDT enhancement indicated slower degradation of the material compared with MCC without PSM. The less solid fraction after the analysis indicated less formation of ash in the earliest stages of degradation (Fig. 12).

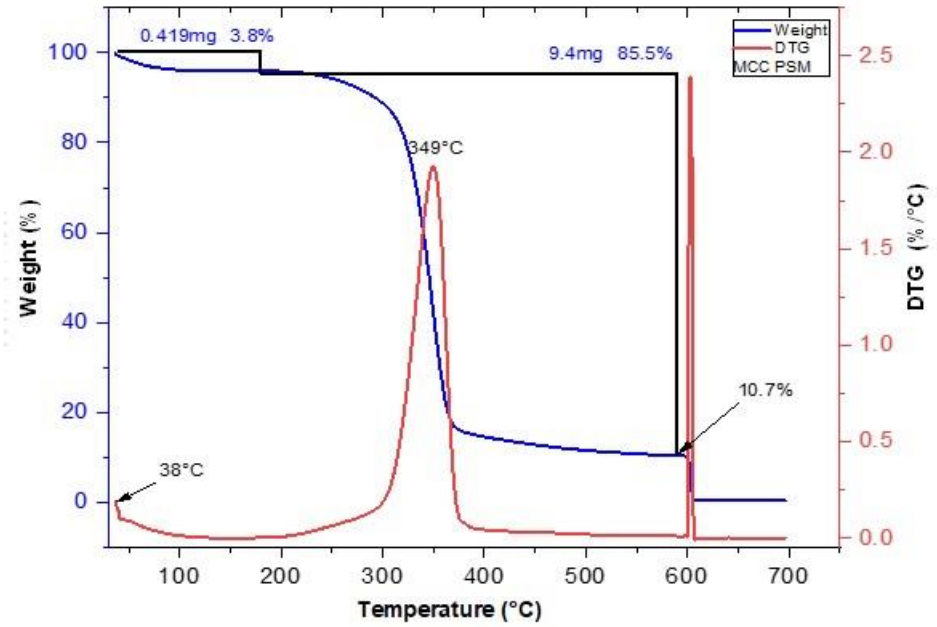


**Fig. 12.** TGA of MCC PSM

## CONCLUSIONS

1. The microcrystalline cellulose (MCC) isolation procedures resulted in cellulose type I (native cellulose) without structural modification. In the sample with NaOH there were no relevant changes. Therefore, the neutralization of MCC did not result in structural damage.
2. The incorporation of NaOH did not alter the Fourier transform infrared (FTIR) absorbance bands detected with any other functional group. Thus, the base reacted selectively with the sulfate groups onto the surface, producing $H_2O$ as a byproduct.
3. Heat drying resulted in agglomeration due to capillarity forces.
4. The characterization brings information about the mechanism of size reduction and the parameters control makes it possible to distinguish the 4 phenomena involved in the fracture mechanism: acid concentration, temperature of drying, sulfation of the surface and ultrasonication.
5. After plasma surface modification (PSM), the MCC showed less crystallinity, but there were no new phases formed by PSM; thus, PSM will enhance coupling without unexpected structural changes.
6. The neutralization with NaOH improved thermal resistances compared to sulfated MCC, thus maintaining the flame-retardant property.
7. Thermogravimetric analysis (TGA) results suggested changes in the thermal resistance of the material after PSM with higher peak temperature of degradation.
8. The fewer deep defects are expected to be favorable to the adhesion mechanism of mechanical interlocking for the synthesis of hybrid composites with thermoplastic matrices.
9. After the morphological, structural, and infrared spectroscopy, the proposed mechanism of fracture and their control of parameters can enhance the coupling of MCC with thermoplastic matrices.

## REFERENCES CITED

Alanis, A., Valdés, J. H., María Guadalupe, N. V., Lopez, R., Mendoza, R., Mathew, A. P., Díaz De León, R., and Valencia, L. (2019). "Plasma surface-modification of cellulose nanocrystals: A green alternative towards mechanical reinforcement of ABS," *RSC Advances* 9(30), 17417-17424. DOI: 10.1039/c9ra02451d

Crews, K., Huntley, C., Cooley, D., Phillips, B., and Curry, M. (2016). "Influence of cellulose on the mechanical and thermal stability of ABS plastic composites," *International Journal of Polymer Science* 2016(10). DOI: 10.1155/2016/9043086

Espino-Pérez, E., Bras, J., Ducruet, V., Guinault, A., Dufresne, A., and Domenek, S. (2013). "Influence of chemical surface modification of cellulose nanowhiskers on thermal, mechanical, and barrier properties of poly(lactide) based bionanocomposites," *European Polymer Journal* 49(10), 3144-3154. DOI: 10.1016/J.EURPOLYMJ.2013.07.017

González-Velázquez, J. L. (2021). "General concepts of mechanical behavior and fracture," in: *A Practical Approach to Fracture Mechanics*, pp. 1-34. DOI: 10.1016/B978-0-12-823020-6.00001-3

Huang, B., He, H., Meng, S., and Jia, Y. (2019). "Optimizing 3D printing performance of acrylonitrile-butadiene-styrene composites with cellulose nanocrystals/silica nanohybrids," *Polymer International* 68(7), 1351-1360. DOI: 10.1002/pi.5824

Kale, R. D., Bansal, P. S., and Gorade, V. G. (2018). "Extraction of microcrystalline cellulose from cotton sliver and its comparison with commercial microcrystalline cellulose," *Journal of Polymers and the Environment* 26(1), 355-364. DOI: 10.1007/s10924-017-0936-2

Kerche, E. F., Neves, R. M., Ornaghi, H. L., Zattera, A. J., and Schrekker, H. S. (2022). "The influence of ionic liquid concentration on microcrystalline cellulose modification," *Carbohydrate Polymer Technologies and Applications* 3, article 100211. DOI: 10.1016/J.CARPTA.2022.100211

Leão, R. M., Jesus, L. C. C., Bertuoli, P. T., Zattera, A. J., Maia, J. M. L. L., del Menezzi, C. H. S., Amico, S. C., and da Luz, S. M. (2020). "Production and characterization of cellulose nanocrystals/ acrylonitrile butadiene styrene nanocomposites," *Journal of Composite Materials* 54(27), 4207-4214. DOI: 10.1177/0021998320927773

Morán, J. I., Alvarez, V. A., Cyras, V. P., and Vázquez, A. (2008). "Extraction of cellulose and preparation of nanocellulose from sisal fibers," *Cellulose* 15(1), 149-159. DOI: 10.1007/s10570-007-9145-9

Mørch, K. A. (2015). "Cavitation inception from bubble nuclei," *Interface Focus* 5(5), article 20150006. Royal Society of London. DOI: 10.1098/rsfs.2015.0006

Oh, S. Y., Yoo, D. il, Shin, Y., and Seo, G. (2005). "FTIR analysis of cellulose treated with sodium hydroxide and carbon dioxide," *Carbohydrate Research* 340(3), 417-428. DOI: 10.1016/j.carres.2004.11.027

Oun, A. A., and Rhim, J. W. (2015). "Effect of post-treatments and concentration of cotton linter cellulose nanocrystals on the properties of agar-based nanocomposite films," *Carbohydrate Polymers* 134, 20-29. DOI: 10.1016/J.CARBPOL.2015.07.053

Pambudi, A. B., Priyangga, A., Hartanto, D., and Atmaja, L. (2021). "Intramolecular hydrogen bond and vibrational spectroscopic study of cellulose oligosaccharide using density functional theory," AIP Conference Proceedings, 2349. DOI: 10.1063/5.0054693

Peng, Y., Gardner, D. J., and Han, Y. (2012). "Drying cellulose nanofibrils: In search of a suitable method," *Cellulose* 19(1), 91-102. DOI: 10.1007/s10570-011-9630-z

Ponsuriyaprakash, S., Udhayakumar, P., and Pandiyarajan, R. (2020). "Experimental investigation of ABS matrix and cellulose fiber reinforced polymer composite materials," *Journal of Natural Fibers*. DOI: 10.1080/15440478.2020.1841065

Qiao, C., Chen, G., Zhang, J., and Yao, J. (2016). "Structure and rheological properties of cellulose nanocrystals suspension," *Food Hydrocolloids* 55, 19-25. DOI: 10.1016/j.foodhyd.2015.11.005

Sèbe, G., Ham-Pichavant, F., Ibarboure, E., Koffi, A. L. C., and Tingaut, P. (2012). "Supramolecular structure characterization of cellulose II nanowhiskers produced by acid hydrolysis of cellulose I substrates," *Biomacromolecules* 13(2), 570-578. DOI: 10.1021/bm201777j

Segal, L., Creely, J. J., Martin, A. E., and Conrad, C. M. (1952). "Opportunity for new developments in all phases of textile manufacturing. ' Literature Cited An Empirical Method for Estimating the Degree of Crystallinity of Native Cellulose Using the X-

Ray Diffractometer," in: *Apparel Manufacturing*, Vol. 43. DOI:10.1177/004051755902901003

Shaik, S., Danovich, D., Silvi, B., Lauvergnat, D. L., and Hiberty, P. C. (2005). "Charge-shift bonding—A class of electron-pair bonds that emerges from valence bond theory and is supported by the electron localization function approach," *Chemistry - A European Journal* 11(21), 6358-6371. DOI: 10.1002/chem.200500265

Shaik, S., Danovich, D., Wu, W., and Hiberty, P. C. (2009). "Charge-shift bonding and its manifestations in chemistry," *Nature Chemistry* 1(6), 443-449. DOI: 10.1038/nchem.327

Spoljaric, S., Genovese, A., and Shanks, R. A. (2009). "Polypropylene–microcrystalline cellulose composites with enhanced compatibility and properties," *Composites Part A: Applied Science and Manufacturing* 40(6–7), 791-799. DOI: 10.1016/J.COMPOSITESA.2009.03.011

Trache, D., Hussin, M. H., Haafiz, M. K. M., and Thakur, V. K. (2017). "Recent progress in cellulose nanocrystals: Sources and production," in: *Nanoscale*, Vol. 9, Issue 5, pp. 1763-1786. Royal Society of Chemistry. DOI: 10.1039/c6nr09494e

Trache, D., Hussin, M. H., Hui Chuin, C. T., Sabar, S., Fazita, M. R. N., Taiwo, O. F. A., Hassan, T. M., and Haafiz, M. K. M. (2016). "Microcrystalline cellulose: Isolation, characterization and bio-composites application—A review," *International Journal of Biological Macromolecules* 93, 789-804. DOI: 10.1016/J.IJBIOMAC.2016.09.056

Trilokesh, C., and Uppuluri, K. B. (2019). "Isolation and characterization of cellulose nanocrystals from jackfruit peel," *Scientific Reports* 9(1). DOI: 10.1038/s41598-019-53412-x

Voronova, M. I., Zakharov, A. G., Kuznetsov, O. Y., and Surov, O. v. (2012). "The effect of drying technique of nanocellulose dispersions on properties of dried materials," *Materials Letters* 68, 164-167. DOI: 10.1016/J.MATLET.2011.09.115

Wu, W., Gu, J., Song, J., Shaik, S., and Hiberty, P. C. (2009). "The inverted bond in [1.1.1]propellane is a charge-shift bond," *Angewandte Chemie* 121(8), 1435-1438. DOI: 10.1002/ange.200804965

Article submitted: November 7, 2022; Peer review completed: December 10, 2022; Revised version received and accepted: December 31, 2022; Published: January 19, 2023.
DOI: 10.15376/biores.18.1.1788-1802